Estuarine Boundary Layer Mixing Processes: Insights from Dye Experiments*

ROBERT J. CHANT
Institute of Marine and Coastal Sciences, Rutgers, The State University of New Jersey, New Brunswick, New Jersey

WAYNE R. GEYER
Woods Hole Oceanographic Institution, Woods Hole, Massachusetts

ROBERT HOUGHTON
Lamont-Doherty Earth Observatory, Columbia University, New York, New York

ELIAS HUNTER
Institute of Marine and Coastal Sciences, Rutgers, The State University of New Jersey, New Brunswick, New Jersey

JAMES LERCZAK+
Woods Hole Oceanographic Institution, Woods Hole, Massachusetts

(Manuscript received 18 September 2005, in final form 12 September 2006)

ABSTRACT

A series of dye releases in the Hudson River estuary elucidated diapycnal mixing rates and temporal variability over tidal and fortnightly time scales. Dye was injected in the bottom boundary layer for each of four releases during different phases of the tide and of the spring–neap cycle. Diapycnal mixing occurs primarily through entrainment that is driven by shear production in the bottom boundary layer. On flood the dye extended vertically through the bottom mixed layer, and its concentration decreased abruptly near the base of the pycnocline, usually at a height corresponding to a velocity maximum. Boundary layer growth is consistent with a one-dimensional, stress-driven entrainment model. A model was developed for the vertical structure of the vertical eddy viscosity in the flood tide boundary layer that is proportional to u_*^2/N_∞, where u_* and N_∞ are the bottom friction velocity and buoyancy frequency above the boundary layer. The model also predicts that the buoyancy flux averaged over the bottom boundary layer is equal to $0.06N_\infty u_*^2$ or, based on the structure of the boundary layer equal to $0.1N_{\mathrm{BL}}u_*^2$, where N_{BL} is the buoyancy frequency across the flood-tide boundary layer. Estimates of shear production and buoyancy flux indicate that the flux Richardson number in the flood-tide boundary layer is 0.1–0.18, consistent with the model indicating that the flux Richardson number is between 0.1 and 0.14. During ebb, the boundary layer was more stratified, and its vertical extent was not as sharply delineated as in the flood. During neap tide the rate of mixing during ebb was significantly weaker than on flood, owing to reduced bottom stress and stabilization by stratification. As tidal amplitude increased ebb mixing increased and more closely resembled the boundary layer entrainment process observed during the flood. Tidal straining modestly increased the entrainment rate during the flood, and it restratified the boundary layer and inhibited mixing during the ebb.

1. Introduction

In recent years numerous studies have characterized tidal period variability of vertical mixing in estuarine environments (Lu et al. 2000; Peters and Bokhorst 2000; Peters 1997; Rippeth et al. 2002; Simpson et al. 2002; Stacey et al. 1999; Stacey and Ralston 2005; Trowbridge et al. 1999; Geyer et al. 2000). Simpson et al. (1990) introduced the phenomenon of tidal straining in which vertically sheared tidal current interacts with the along-channel density gradient. Tidal straining was found to augment stratification during the ebb and reduce it during the flood, contributing to the now familiar tidal asymmetry in vertical mixing (Jay and Smith 1990). Turbulence measurements by Peters and Bokhorst (2000) and Trowbridge et al. (1999) provided direct confirmation of tidal asymmetry in turbulence; they also found significant spring–neap variations in the

* Lamont-Doherty Earth Observatory Contribution Number 7035.

+ Current affiliation: College of Oceanic and Atmospheric Sciences, Oregon State University, Corvallis, Oregon.

Corresponding author address: Robert Chant, IMCS, Rutgers University, 71 Dudley Road, New Brunswick, NJ 08901-8521.
E-mail: chant@marine.rutgers.edu

DOI: 10.1175/JPO3088.1

asymmetry, with greater asymmetry occurring during neap tides. Similar findings were obtained by Geyer et al. (2000) based on an analysis of the estuarine momentum balance.

Although considerable attention has been focused on turbulent stress and dissipation of turbulent kinetic energy in estuaries (e.g., Rippeth et al. 2002; Stacey and Ralston 2005; Stacey et al. 1999; Peters and Bokhorst 2000; Trowbridge et al. 1999), the quantification of vertical salt flux (or, equivalently, buoyancy flux) has been more limited. Peters and Bokhorst (2000) made estimates of buoyancy flux using the Osborn (1980) relation based on a local turbulent kinetic energy balance. This method requires an a priori estimate of the flux Richardson number, which they derive from laboratory measurements and earlier field studies.

Another approach to obtaining buoyancy flux estimates is to quantify the vertical spreading of a deliberate tracer, such as dye or SF_6. Tracer studies of buoyancy flux have the advantage that they do not require a priori assumptions about the turbulence. Ledwell et al. (1993) provided an accurate estimate of the mixing rate in the thermocline of the North Atlantic with SF_6, and similar methods have been used in coastal waters with Rhodamine and Fluorescein dye (Sundermeyer and Ledwell 2001; Ledwell et al. 2004; Houghton et al. 2004). In this paper we present the results of a set of dye tracer releases in the Hudson River estuary to quantify the vertical mixing rate in different conditions through the tidal cycle and spring–neap cycle of tidal amplitude. Section 2 describes the dye experiments while section 3 characterizes the tidal period and spring–neap variations in mixing observed with the dye tracer. In section 4a we focus on flood tide mixing and show that boundary layer growth occurs due to entrainment and that this growth rate is consistent with the Trowbridge (1992) model. In section 4a we also access the relative roles of entrainment and tidal straining to boundary layer growth. This is followed by analysis that quantifies vertical mixing rates and relates vertical eddy diffusivity to the bottom friction velocity and overlying stratification. In section 4b ebb boundary layer mixing is discussed and in section 4c we provide estimates of the vertical salt flux and of the flux Richardson number. Conclusions are drawn in section 5.

2. The dye experiments

The dye studies were conducted in the Hudson River estuary in May 2002 in a reach north of the George Washington Bridge (Fig. 1) that is relatively uniform in the along-channel direction. The channel is laterally asymmetric, with a 15-m-deep channel running close to its eastern shore and a shoaling western flank. The mean river discharge (measured at Green Island Dam, near Troy, New York) during May 2002 was 811 $m^3 s^{-1}$, about 20% above average (Fig. 2). There was a peak flow of around 2000 $m^3 s^{-1}$ between the two sets of dye releases (shown as horizontal bars on Fig. 2). Tidal range was at its fortnightly minimum (neap) during the first release (Fig. 2), low but increasing during the second release, sharply increasing during the third release, and near its maximum during the fourth release (spring). Stratification was strongest during the first release and transitioned from highly stratified to nearly mixed during the third release (Fig. 2). The most comprehensive surveys were conducted following the first and third releases, so the main focus of this paper is on them, with some supporting data from the other releases.

The dye studies were complemented with moored instruments that included four 1.2-MHz Acoustic Doppler Current Profilers (ADCP) deployed across the channel approximately 3 km north of the George Washington Bridge (Fig. 1). The mooring array also included 12 Seabird CT sensors and 2 Paroscientific pressure sensors. The mooring array was deployed on 22 April and recovered on 6 June. Lerczak et al. (2006) provide a detailed description of this mooring array. We refer to the moorings as sites 1 through 4 from west to east.

Each of the dye studies commenced with an injection of ~40 kg of Fluorescein dye into the bottom mixed layer in the deep channel on the eastern side of the river. The initial dye streak was several hundred meters long in the cross-channel direction, running between the 10-m isobaths. Each release took approximately 15 min. Following the release, the dye patch was surveyed by two boats. One boat ran along-channel sections and the second boat ran cross-channel sections. The cross-channel surveys were done in tow-yo mode (i.e., continuous vertical profiling while underway at approximately 3 kt) and provided ~50 m spatial resolution of the cross-channel structure of the dye. Typically each patch survey involved four to six cross-channel sections. The along-channel surveys were completed with approximately 10–15 profiles and thus the spatial resolution of the along-channel surveys decreased with increasing patch size. Patch surveys took approximately 1 h to complete. The injection site was selected so that during the first tidal cycle after injection the dye patch would pass through the mooring array while still remaining north of the more complicated channel morphology south of the George Washington Bridge (Chant and Wilson 1997, 2000) at river kilo-

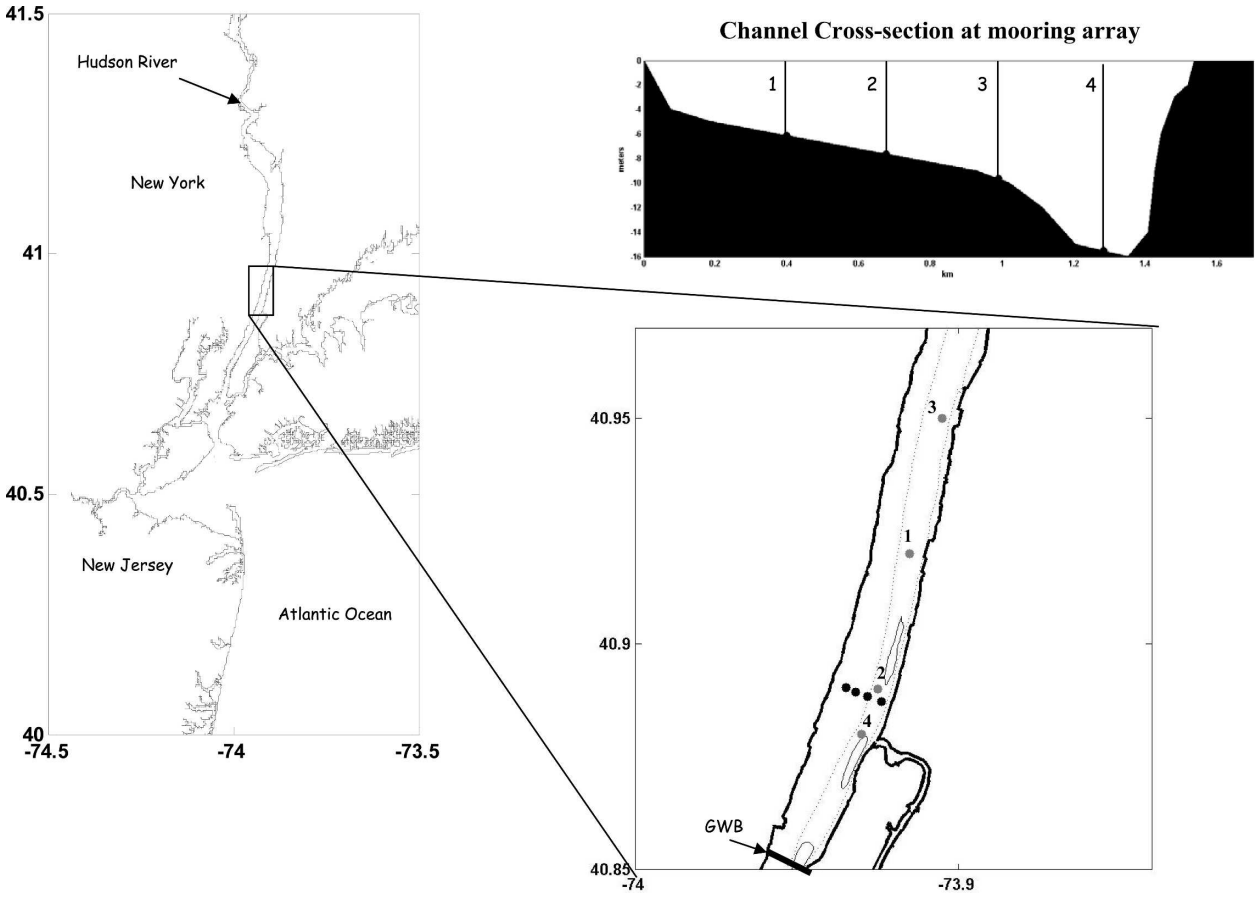

FIG. 1. Study site. In the small-scale map the black dots show mooring sites. Gray dots show locations of dye releases. Release 1 and 3 occurred at slack before ebb on 5 and 22 May, respectively. Release 2 and 4 occurred during early flood on 9 and 24 May. Dashed lines are the 10-m isobath, and closed solid lines the 15-m isobath. Upper right insert depicts channel cross section at mooring array and locations of moorings.

meter 18. Each boat was equipped with a 1200-kHz RDI acoustic Doppler profiler (ADCP) and an Ocean Sensor CTD (OS-200) that was mated with a Chelsea Aquatracka III fluorometer for dye tracking. Both the CTD and fluorometer operated at approximately 6 Hz. One day prior to each dye injection we conducted a CTD survey of the estuary to the inland limit of salt.

Over the course of the four dye experiments we completed 29 dye-patch surveys. While the mean inventory of these patches was only 25.2 kg, significantly less than the amount injected, the standard deviation was only 3.9 kg. We suspect the reduced mean inventory may be due to fluorometer calibration. Nevertheless, the patch-to-patch consistency in dye inventory allows us to evaluate the changing properties of the dye patch.

The variations of current and salinity through the course of the dye study are shown in Fig. 3. Near-bottom currents (1.5 m above bottom) were typically 0.5 m s^{-1} during neaps and up to 0.9 m s^{-1} during springs. Surface currents showed less spring–neap variation, sometimes reaching 1.5 m s^{-1} on strong ebbs during both springs and neaps. As noted above, salinity stratification was strong during the first two releases and transitioned from strongly stratified to mixed conditions during the third release.

3. Results

a. Neap conditions

The 5 May injection occurred during early ebb. The injection was about 2 m above the bottom in the boundary layer, at a target salinity of 17.1 psu. Surface-to-bottom salinity difference exceeded 15 psu at the time of injection. Along-estuary sections through the patch are shown in Fig. 4 and vertical profiles in Fig. 5. The first panel in each figure corresponds to maximum ebb, then early, mid-, and late flood conditions on the day of the injection. During maximum ebb the bulk of the patch resided near the bottom, although there was some penetration into the lower halocline. The highest

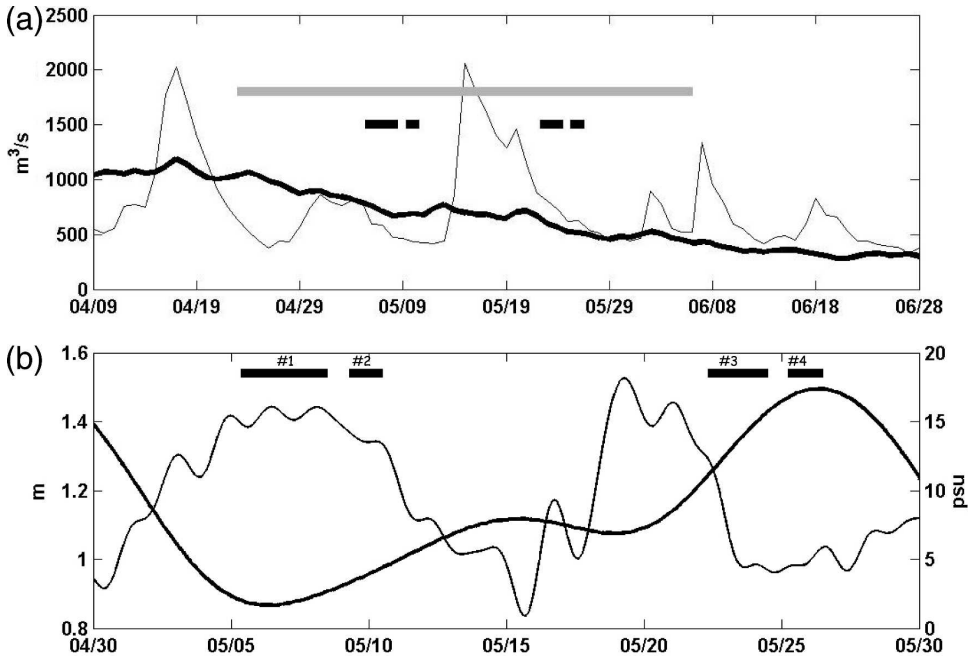

FIG. 2. (a) Thick line shows mean daily discharge based on a 56-yr record at Green Island. Thin line shows discharge at Green Island in 2002. Gray line depicts duration of mooring deployment and black dashes depict the duration of each dye experiment. (b) Tidal range at the Battery (thick line) and subtidal surface to bottom salinity difference from mooring 4 (thin line). Thick black dashes depict duration of each dye experiment.

concentrations of dye patch remained at the bottom within a few kilometers of the injection site (kilometer 25).

During flood (Figs. 4b–d and 5b–d), the dye patch thickened as the bottom boundary layer grew. At the beginning of the flood, the patch was about 2.5 m thick and increased to 6.5 m by the end of the flood. The upper limit of the dye patch corresponded closely to the location of the velocity maximum, which indicates the upper limit of the influence of bottom stress on momentum.

The average salinity within the dye patch decreased through the flood, indicating the vertical entrainment of lower-salinity water into the bottom boundary layer. The rate of freshening was found to be consistent with one-dimensional vertical mixing, as will be demonstrated in section 4a(2). The salinity structure did not show a distinctive change at the top of the boundary layer (defined here by the upper limit of the dye)—there was a continuous increase in salinity gradient, reaching a local maximum near the upper limit of the dye (Fig. 5, left panels). Clearly the boundary layer was not a mixed layer, but rather a stratified shear layer with vertically varying gradients.

The gradient Richardson number (Ri) reached values close to 0.25 within the dye patch during the strong ebb as well as during the strong flood, although its average value within the boundary layer was around 0.5 (Fig. 5, first and third panels). During decreasing flow conditions, Ri increased and became variable.

The lateral distribution of dye (Fig. 6) indicates that the dye was confined to the deep, eastern part of the channel during the ebb, but it spread across the channel during the flood. Once the dye spread to occupy the channel, the lateral variations of dye were modest, roughly corresponding to lateral variations in salinity. There was more lateral variability at the landward and seaward limits of the patch, reflecting differential advection.

The 9 May release occurred during flood, when the dye was injected into the bottom boundary layer at a target salinity of 18 psu. Stratification and near-bottom tidal current velocities during this experiment were similar to those during the 5 May release (Fig. 3), although there was an increase in surface currents during flood at the diurnal period. The 9 May experiment provided detailed estimates of mixing during the ebb and complements the 5 May experiment that better resolved the flood. Together these two experiments reveal that during neap tide the boundary layer, as defined by the properties of the core of the dye patch, freshens more rapidly during flood tide than on ebb

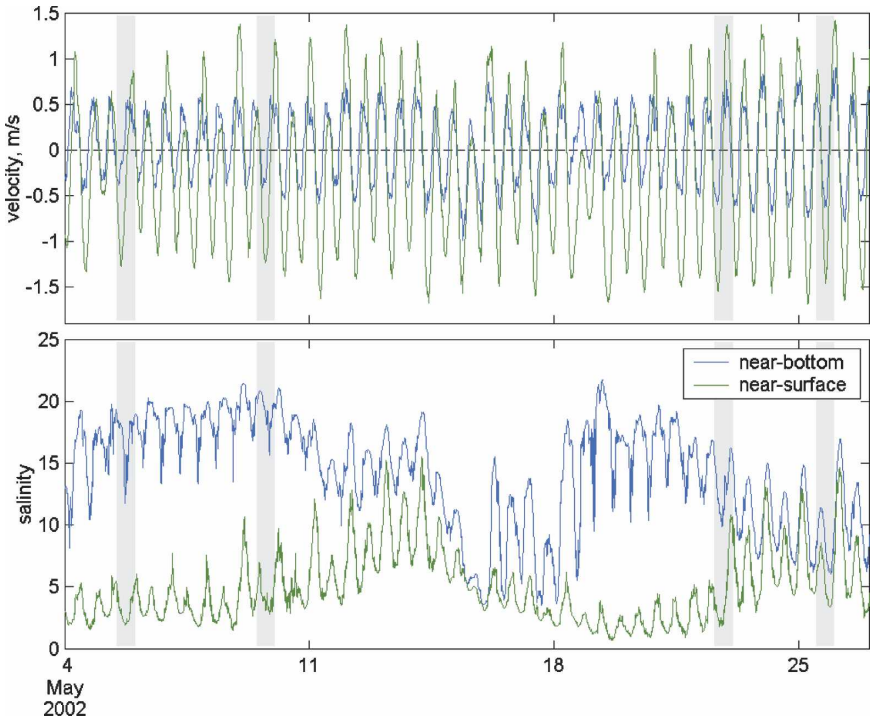

FIG. 3. (top) Near-surface (green) and near-bottom (blue) currents from mooring site 4. Flooding current is positive. (bottom) Near-surface (green) and near-bottom (blue) salinity from mooring site 4. See Fig. 1 for locations of moorings.

(Fig. 7a). Details of defining the core of the dye patch are given in section 4a(1).

b. Neap-to-spring transition

The 22 May injection occurred just prior to a rapid decrease in stratification approaching spring tides. The dye was injected into the bottom boundary layer at a mean salinity of 12.2 psu at slack before ebb. Like the first injection the rate of freshening during the ebb was weaker than during the flood. Furthermore, the vertical distribution of dye showed multiple peaks that indicate advective as well as diffusive processes (Fig. 8a). The highest concentrations were not near the bottom, which can only be explained by vertical advection and/or secondary circulation. As the ebb progressed a broad mixing layer developed over the bottom 6 to 8 m, evident both in the dye distribution and the salinity profile. This indicates that boundary layer mixing began to dominate over vertical advection in controlling the vertical distribution of the dye.

During flood the vertical extent of the dye patch was clearly limited by the velocity maximum (Fig. 8b). The velocity, salinity, and dye distributions within the boundary layer were similar to the neap case, but the boundary layer grew significantly more rapidly. The dye patch continued to freshen during the flood and mixed both horizontally and vertically through isohalines. At the beginning of flood the near-bottom salinity at the core of the dye patch was at 11 psu, while by the end of flood the near-bottom salinity in the core had decreased to 9 psu. Again, this indicates the influence of entrainment of overlying lower-salinity fluid. The Richardson numbers in the boundary layer were consistently at or below 0.25 during the flood, except near the velocity maximum where they increased to around 1.

A 24 May injection occurred during spring tides. Dye was injected near the bottom at a target salinity of 7 psu and top-to-bottom salinity stratification was weak and less than 2 psu (Fig. 3). The spring tide currents in the presence of weak stratification rapidly mixed the dye throughout the water column. Consequently, these data were not suitable to characterize boundary layer growth because the boundary layer occupied the entire water column for most of the experiment.

4. Discussion

a. Mixing on flood

1) BOTTOM BOUNDARY LAYER GROWTH

The following analysis quantifies the extent that entrainment, rather than vertical advection, drives the

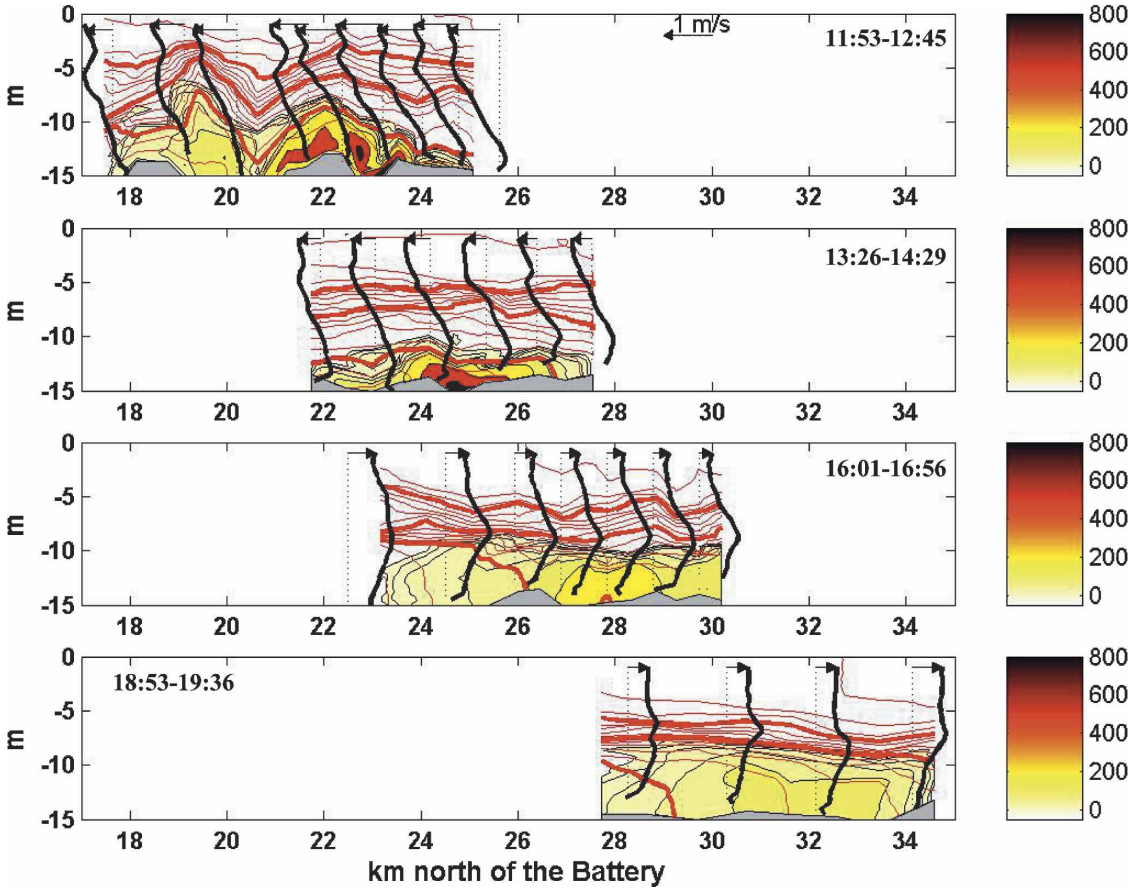

FIG. 4. Along-channel sections across dye patch on 5 May salinity (red contour), velocity profile (thick black line), and dye concentration (filled contours). The dye is contoured at 5, 10, 20, 50, 100, 200, 500, and 800 parts per 10^{11}. The thicker salinity contours are the 5-, 10-, and 15-psu isohalines. Velocity profiles are shown for every other CTD/dye profile. Dashed line is zero velocity and vector depicts near-surface velocity. Panels are taken during maximum ebb, early flood, peak flood, and late flood. Times are eastern daylight time. The injection occurred at kilometer 25.

vertical growth rate of the dye patch. This analysis required estimates of the growth and freshening rate of the dye. This was done for both the properties within the core of the dye patch and with patch-mean properties. Results from these two approaches reached similar results and therefore we only present the analysis on the relatively homogenous core of the dye patch. The core of each patch was defined by selecting only profiles with maximum dye concentrations greater than e^{-1} times the maximum dye concentration in the patch. For each of these profiles the top of the dye patch was defined as the depth where dye concentration was 10% of the maximum dye concentration for each cast. Because of the sharp vertical gradients at the top of the dye patch and the self-similarity of the vertical structure of the dye (see, e.g., Fig. 12) these estimates of boundary layer height were relatively insensitive to reasonable changes in the 10% criteria.

During flood there was a period of nearly steady boundary layer growth. The mean boundary layer height of the core of the patch grew at a rate of 1.9×10^{-4} m s^{-1} during the neap tide experiment (5 May) and 3.8×10^{-4} m s^{-1} during the stronger tidal conditions on 22 May (Fig. 9a). Boundary layer growth, however, could be due to horizontal convergence and/or vertical entrainment. To determine the relative role of flow convergence to entrainment the volume-integrated salt within the core of the dye patch were evaluated. Mixing causes its volume to increase monotonically with time, and an entrainment velocity can be defined that represents the normal velocity of that volume (which is typically oriented vertically). The conservation of volume of the dye patch can be written as

$$\frac{dV}{dt} = A_p w_e, \tag{1}$$

where V is the volume of fluid that contains dye, A_p is the surface area of that concentration "surface," and w_e

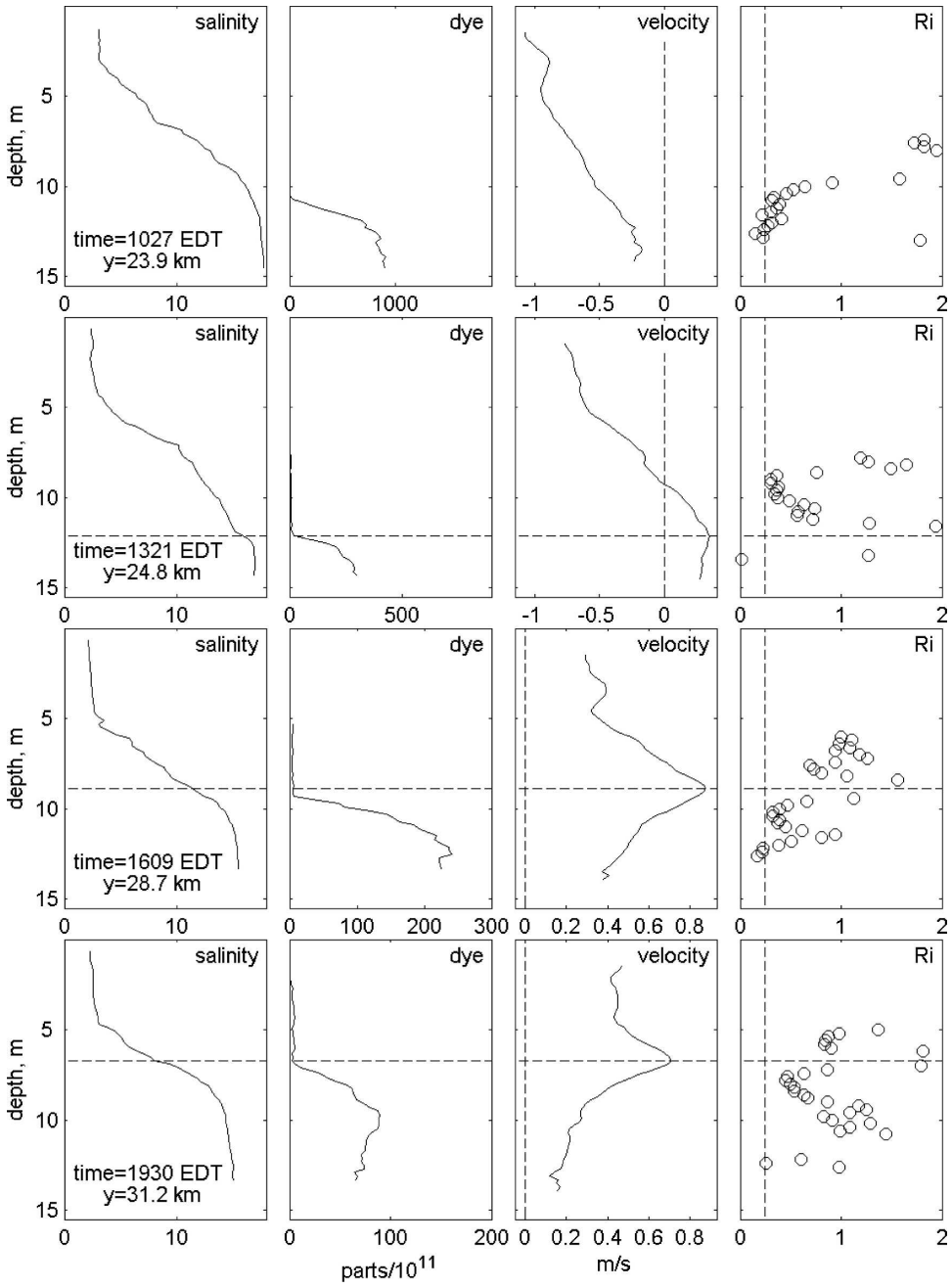

FIG. 5. Profiles of salinity, dye concentration, along-channel velocity, and Richardson numbers during first tidal cycle following the 5 May (neap tide) injection. Profiles are obtained from shipboard observations. Flooding current is positive. Horizontal dashed lines depict the top of the boundary layer. Vertical dashed lines in velocity profiles is at 0 m s^{-1}. Vertical dashed line in Richardson number plots is at 0.25.

is the area-averaged outward velocity of that surface relative to the local water, or the "entrainment velocity" of water into the dye patch. The quotes are used because the term entrainment is used in many different contexts. What is meant here is that, in a reference frame that moves with the diffusing dye on a constant isopleth, there is a net fluid motion toward higher dye concentration. The more conventional use of the term entrainment applies to the conditions during the flooding tide in which there is an abrupt change in turbulent intensity at the top of the boundary layer corresponding to a sharp drop in dye concentration. If the patch of dye

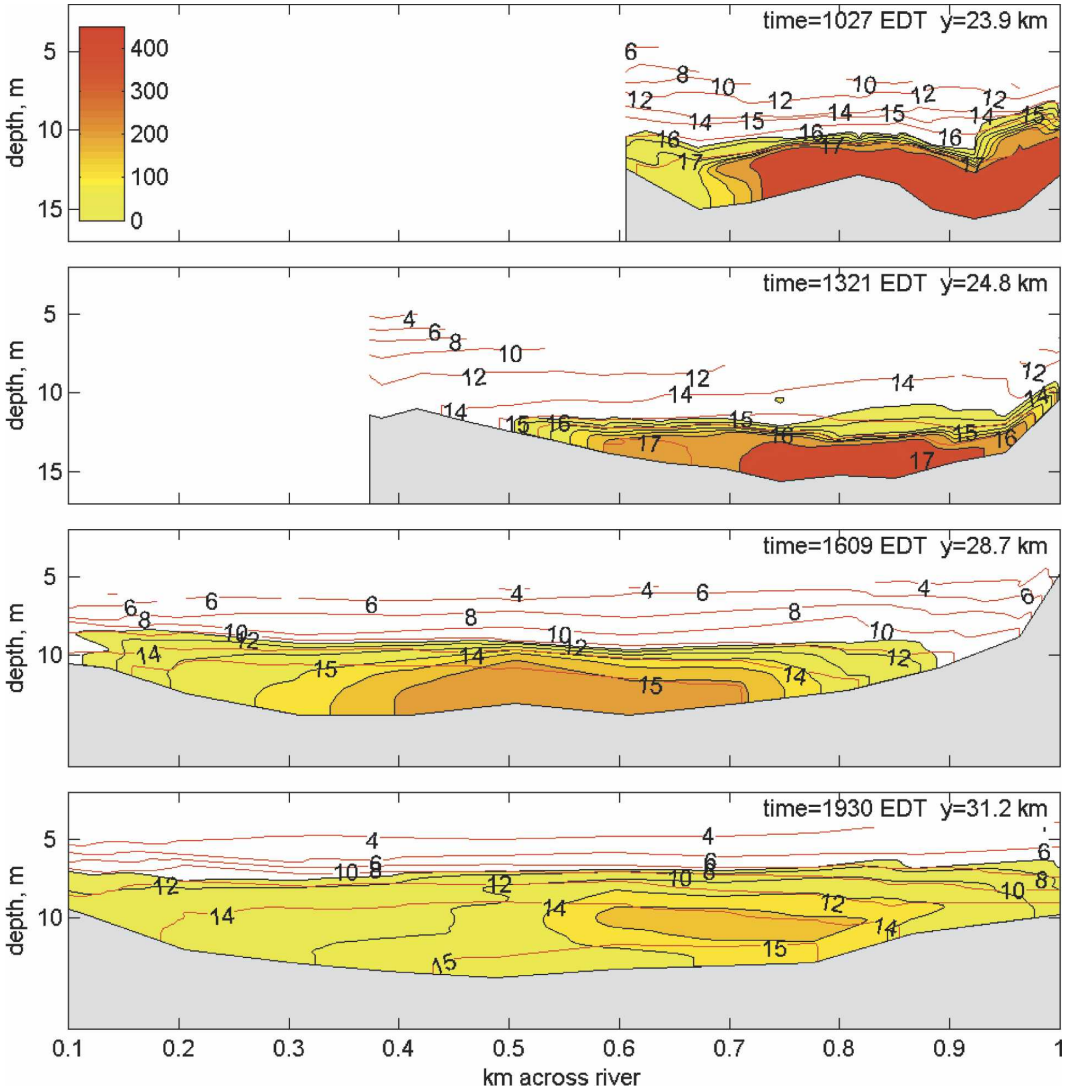

FIG. 6. Cross-channel sections across center of dye patch during the flood tide on 5 May. Color is dye concentration and salinity is red contour.

touches the bottom everywhere, then the surface across which the entrainment occurs is only the upper surface, and it is approximately equal to the horizontal projected area of the dye patch A_h. These are the conditions, particularly related to the flood tide conditions, that will be considered in this analysis. The average thickness of the dye patch is defined simply by $\bar{h} = V/A_h$, and the time rate of change of the height is

$$\frac{d\bar{h}}{dt} = \frac{1}{A_h}\frac{dV}{dt} - \frac{V}{A_h^2}\frac{dA_h}{dt}. \tag{2}$$

The first term on the right-hand side is the entrainment term, and the second is the change in patch thickness associated with horizontal convergence or divergence of the patch. Equation (2) can be rewritten as

$$\frac{d\bar{h}}{dt} = w_e + w_a, \tag{3}$$

where, again, w_e is the entrainment velocity and w_a is vertical advection. Note that w_e must be positive, as it is associated with the irreversible spreading of the dye patch, whereas w_a can be of either sign depending on the geometry of the flow. Only entrainment, w_e, will cause the dye patch and boundary layer to freshen. Therefore the extent to which the boundary layer growth was driven by entrainment, rather than flow convergence, was determined by a comparison between the freshening rate of the core of the dye patch and $d\bar{h}/dt$. The average salinity within the core of the patch can be related back to the entrainment velocity via the equation

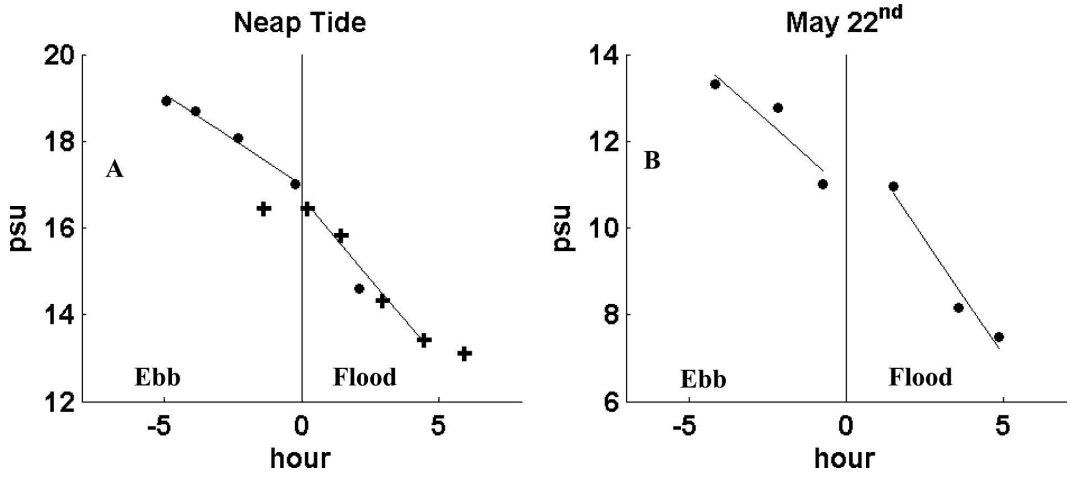

FIG. 7. Mean salinity of core of dye patch (a) during the neap-tide experiments and (b) during transitional experiment. Line is best fit to ebb and flooding freshening rate. For the neap-tide experiments plus signs are for the 5 May data and dots are for 9 May data.

$$\frac{d\bar{s}}{dt} = -\frac{(\bar{s} - s_h)}{\bar{h}} w_e, \tag{4}$$

where $d\bar{s}/dt$ is the time rate of change of salinity following the dye and s_h is the average salinity at the top of the boundary layer, which is being entrained into the patch. Values for the quantities in Eq. (4) are listed in Table 1.

The freshening rate of the core of the dye on 5 May required an entrainment velocity of 2.3×10^{-4} m s^{-1}, consistent with the observed growth rate of 1.9×10^{-4} m s^{-1}. Similarly the requisite entrainment rate on 22 May, based on the freshening rate that day, is 4.1×10^{-4} m s^{-1}, which is roughly consistent with the observed growth rate on flood of 3.8×10^{-4} m s^{-1}. Consequently we conclude that the growth of the bottom boundary layer is almost entirely due to entrainment and has little contribution from a vertically advective process.

Estimates of the patch-mean thickness growth rate and freshening rate were also made. While both growth and freshening rates are about 20%–30% slower than those obtained by the analysis of the patch's core, the results are similar in that they also indicate that boundary layer growth is primarily driven by entrainment. The moderate differences between the properties of the core and the patch mean properties may be due to patch-scale variability in mixing and redistribution by three-dimensional circulation. However, these processes appear to be secondary to the flood tide boundary layer dynamics. We acknowledge that this analysis is two-dimensional and neglects lateral variability in channel depth. The impact of lateral variations in depth on boundary layer processes are discussed after section 4a(2).

2) COMPARISON WITH THE TROWBRIDGE MODEL

Next we compare these growth rates with a boundary layer model developed by Trowbridge (1992) that is an extension of earlier models developed by Kato and Phillips (1969), Kantha et al. (1977), and Price et al. (1986). The model assumes that the Richardson number in the boundary layer is held at the critical value of 0.25 by a balance between shear forcing associated with a surficial stress and buoyancy supplied due to entrainment of pycnocline fluid into the boundary layer. The observations reported here are approximately consistent with the assumption that Ri = 0.25 in the boundary layer. The growth of the boundary layer is written as

$$\frac{\partial \bar{h}}{\partial t} = \frac{\mathrm{Ri}_c^{1/2} \gamma}{N_\infty} \frac{u_*^2}{\bar{h}}, \tag{5}$$

where $\mathrm{Ri}_c = 0.25$ is the critical Richardson number, N_∞, is the buoyancy frequency of the pycnocline, $\bar{h}$ is boundary layer thickness in the *thalweg*, u_* is the friction velocity, and $\gamma = 1.22$ is a constant of integration from Trowbridge (1992). We estimate bottom friction using the quadratic drag law $\tau_b = C_d \rho v |v|$. Based on direct estimates of stress and near-bottom velocities Trowbridge et al. (1999) found $C_d = 0.0017$ in the Hudson applied for currents at $d = 3.5$ m above the bed, which corresponds to a $C_d = 0.0021$ for our near-bottom velocity 1.35 m above the bed. Time series of friction velocity for sites 2, 3, and 4 following the first and third dye injections are shown in Fig. 10. Site 4 is deeper than site 3, which results in stronger baroclinic forcing at site 4, and thus relatively weaker stress during

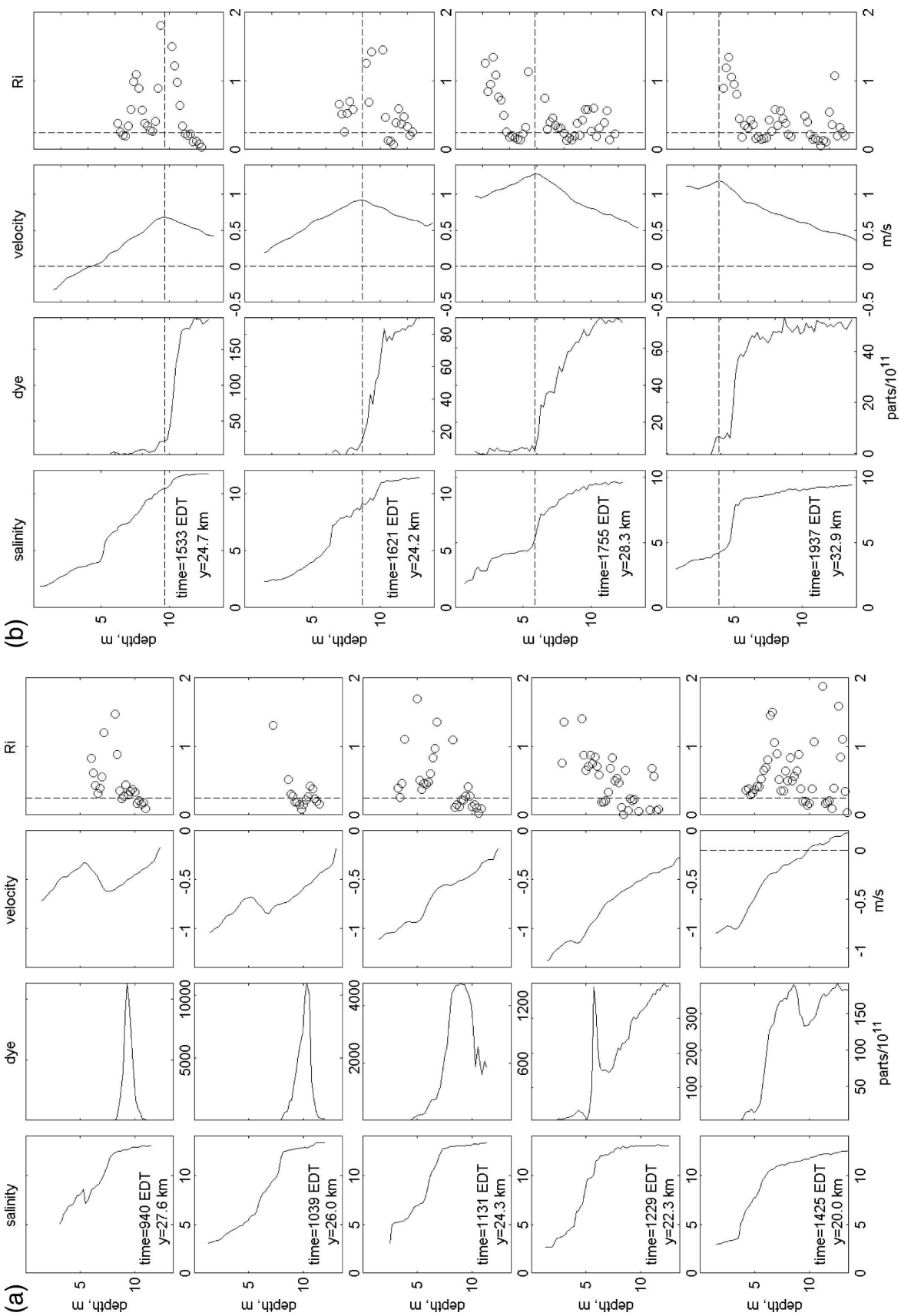
(a)
salinity
dye
velocity
Ri
depth, m
parts/10^11
m/s
time=940 EDT
y=27.6 km
time=1039 EDT
y=26.0 km
time=1131 EDT
y=24.3 km
time=1229 EDT
y=22.3 km
time=1425 EDT
y=20.0 km
(b)
time=1533 EDT
y=24.7 km
time=1621 EDT
y=24.2 km
time=1755 EDT
y=28.3 km
time=1937 EDT
y=32.9 km

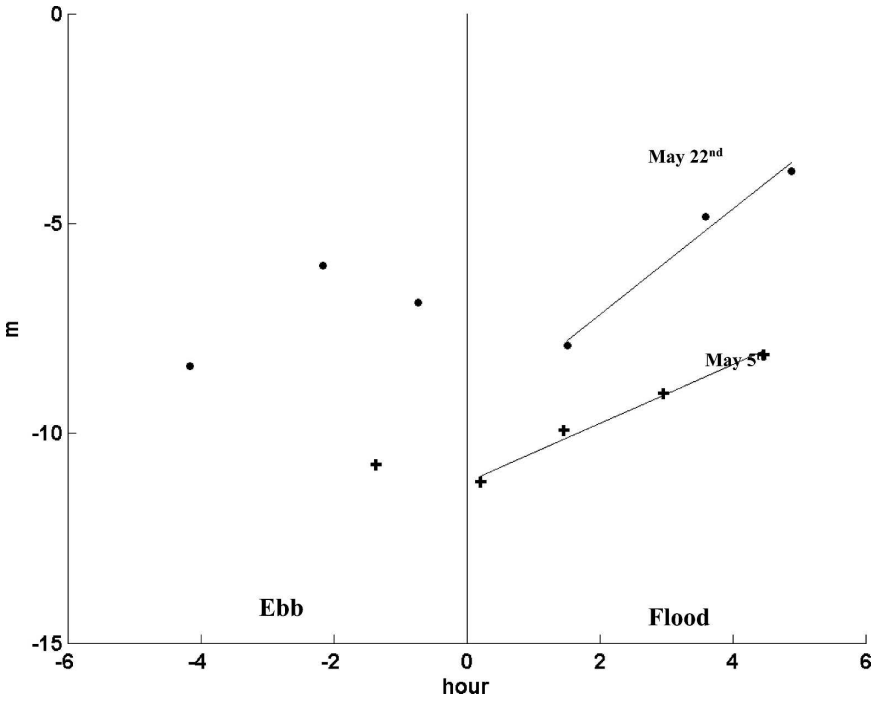

FIG. 9. Height of bottom boundary during the 5 May neap-tide experiment (plus signs) and during the 22 May transitional experiment (dots). Line is best fit to flood-tide boundary layer height during flood.

the ebb. However, during the flood bottom stresses are approximately equal. For the purpose of determining the intensity of mixing during the flood we used the stress estimate from mooring 4. Note that at site 4 the stress was much weaker during the ebb than the flood during neap tides but it became more symmetrical during spring tide conditions. This variation in bottom stress is an important contributor to tidal asymmetry, as will be discussed below. We note that the biggest uncertainty in this comparison our estimates of u_*, which we feel are likely to be accurate to within 20%.

Other variables needed for comparison are the thickness of the boundary layer and the stratification at the top of the boundary layer. The stratification at the top of the layer is taken to be the mean stratification at the top of the core of the dye patch and the thickness of the boundary layer is taken as the mean elevation of the top of the core at midflood, when the estimate of $\partial\bar{h}/\partial t$ is well defined.

In general, the model agrees well with the observed growth of the bottom boundary layer (Table 1). During neap tides the model predicts a growth rate of 1.7×10^{-4} m s^{-1} and the observed growth rate is 1.9×10^{-4} m s^{-1} while during the 22 May experiment both the observed growth rate and the modeled growth rate is 3.8×10^{-4} m s^{-1}. The agreement between the model results and observations provides support for the application of the Trowbridge (1992) entrainment model to these results and further emphasizes the dominance of 1D processes in driving bottom boundary layer evolution. Moreover, these results imply that vertical mixing is primarily accomplished through entrainment processes.

While the above comparison suggests that the Trowbridge model works locally, in reality boundary layer growth will be modified by the lateral variation in bathymetry. As the boundary layer grows vertically, the bottom layer also grows laterally because of the sloping

←

FIG. 8. (a) Profiles of salinity, dye concentration, along-channel velocity, and Richardson numbers during ebb, following the 22 May (transitional) injection. Profiles are obtained from shipboard observations. Flooding current is positive. Vertical dashed lines in velocity profiles are at 0 m s^{-1}. Vertical dashed line in Richardson number plots are at 0.25. (b) Profiles of salinity, dye concentration, along-channel velocity, and Richardson numbers during flood following the 22 May (transitional) injection. Profiles are obtained from shipboard observations. Flooding current is positive. Horizontal dashed lines depict the top of the boundary layer. Vertical dashed lines in velocity profiles are at 0 m s^{-1}. Vertical dashed line in Richardson number plots are at 0.25.

TABLE 1. Parameters used to estimate boundary layer growth rate.

Parameter	5 May	22 May
$\partial\bar{h}/\partial t$ (observed)	0.19 mm s^{-1}	0.38 mm s^{-1}
$\partial\bar{s}/\partial t$	2.1×10^{-4} psu s^{-1}	2.1×10^{-4} psu s^{-1}
$\Delta s = \bar{s} - s_h$	4.5 psu	4 psu
$\bar{h}$	5.0 m	8.0 m
N_∞	0.12 s^{-1}	0.08 s^{-1}
w_e [Eq. (4)]	0.19 mm s^{-1}	0.41 mm s^{-1}
w_e [Eq. (5)]	0.17 mm s^{-1}	0.38 mm s^{-1}
$u_{*\text{flood}}$	1.3 cm s^{-1}	2.0 cm s^{-1}
$u_{*\text{ebb}}$	0.7 cm s^{-1}	1.5 cm s^{-1}
K_z (upper)	3.7 cm^2 s^{-1}	13.2 cm^2 s^{-1}
K_z (max)	18 cm^2 s^{-1}	62 cm^2 s^{-1}

channel. This lateral divergence tends to reduce growth rate because a portion of the increased volume associated with entrainment spreads laterally onto the flank. However, according to Eq. (5), the boundary layer growth rate increases with decreasing boundary layer thickness on the flank and thus tends to compensate for the former effect. The fact that the boundary layer in the *thalweg* appears to grow as fast as (5) predicts indicates that the mean entrainment over the boundary layer exceeds that predicted by (5), and this is consistent with more rapid entrainment on the flank where $\bar{h}$ decreases.

3) THE INFLUENCE OF TIDAL STRAINING ON FLOOD

Tidal straining will also contribute to boundary layer growth. To assess the relative importance of tidal straining to entrainment in driving boundary layer growth we considered an idealized boundary layer of thickness δ and a constant vertical shear with currents zero at the bottom and increasing to Δu at δ (Fig. 11). The boundary layer extends across a mixed bottom layer of thickness δ_M and penetrates into a linearly stratified layer of thickness $d\delta_s$ above (Fig. 11). In this conceptual model the boundary layer advects upstream at $\Delta u/2$, while the stratified top of the boundary layer advances at Δu. Salinity at the top of the boundary layer is $S_M - (\partial s/\partial z)d\delta_s$, where is S_M is the salinity in δ_M (or S_2 in the case of Fig. 11). At the top of the boundary layer tidal straining drives $\partial s/\partial t$ at a rate $(\Delta u/2)\partial s/\partial x$ faster than the mean value of $\partial s/\partial t$ in the boundary layer. Therefore the salinity at the top of the boundary will decrease to S_M in time

$$dt = 2\frac{\partial s}{\partial z}\, d\delta_s \left(\Delta u \frac{\partial s}{\partial x}\right)^{-1},$$

causing the mixed region to grow by $d\delta_s$. Therefore the rate that the boundary layer grows due to tidal straining is

$$\frac{d\delta_s}{dt} = \frac{\Delta u \partial s/\partial x}{2\partial s/\partial z}. \tag{6}$$

Combining Eqs. (5) and (6) we can write an expression for boundary layer growth that includes both entrainment and tidal straining by noting that the Richardson number in the boundary layer is about ¼ and thus $\Delta u = N_{\text{BL}}\delta/\text{Ri}_c^{1/2}$:

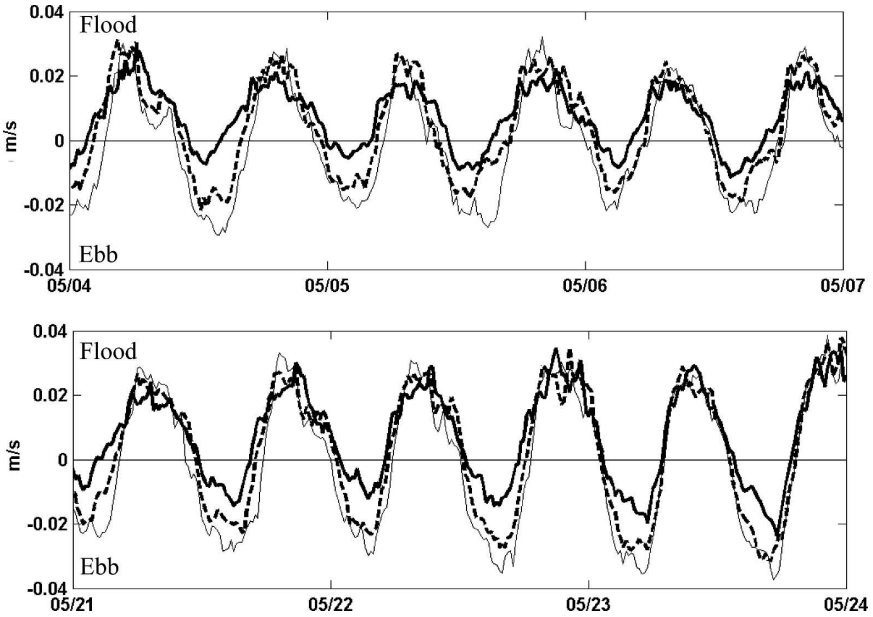

FIG. 10. Estimates of bottom friction velocity during the (top) first and (bottom) third dye experiments. Thick solid line is for site 4, dashed line is for site 3, and thin line is for site 2.

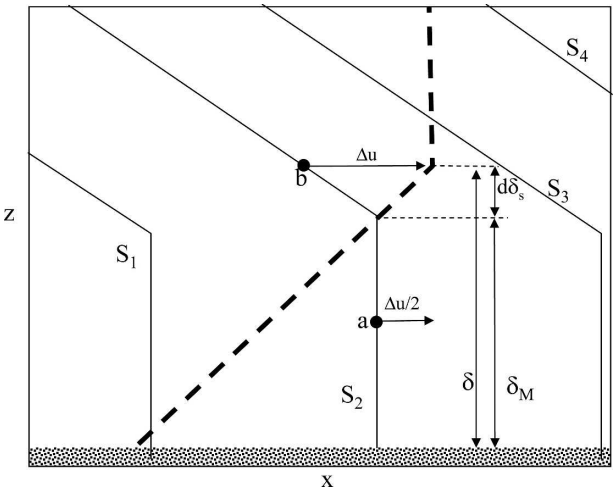

FIG. 11. Conceptual model of tidal straining. Thin solid lines show four isohalines and dashed line depicts velocity profile. Velocity is 0 at the bottom, increases linearly to Δu at δ, and is constant above. The boundary layer is mixed over height δ_M and stratified at higher elevation at across layer of thickness $d\delta_s$. Vertical shear advects point b upstream $\Delta u/2$ faster than point a and causes boundary layer height to increase by $d\delta_s$ when it catches up to point a.

$$\frac{\partial h}{\partial t} = \left(w_e + \frac{\partial \delta_s}{\partial t} \right) = w_e \left(1 + \frac{\varepsilon^2 N_{\mathrm{BL}}}{2\gamma N_\infty \mathrm{Ri}_c} \mathrm{Ri}_x \right), \quad (7)$$

where N_{BL} is the buoyancy frequency in the "mixed" portion of the boundary layer,

$$\mathrm{Ri}_x = \frac{g}{\rho} \frac{\partial \rho}{\partial x} h^2 / u_*^2$$

is the horizontal Richardson number (Stacey and Ralston 2005; Monismith et al. 2002), h is the total water depth, and ε is the fraction of the water column occupied by the bottom boundary layer. The second term on the right-hand side of (7) is the relative contribution of tidal straining to boundary layer growth during flood. (Later in the paper, based on the use of a structure function in the boundary layer, we find that $N_\infty = \sqrt{3} N_{\mathrm{BL}}$, which for $\varepsilon = 0.5$ indicates that this term is approximately equal to 0.2 Ri_x.) In the 5 May experiment the tidal straining term was approximately 0.3, suggesting that tidal straining had a modest contribution to boundary layer growth, while during the 22 May flood it was less than 0.1 and tidal straining was of minimal importance.

In general, however, the close agreement between the entrainment model and the observations suggests that during flood tidal straining plays a secondary role in bottom boundary layer growth, particularly during the 22 May experiment.

4) QUANTIFYING THE VERTICAL STRUCTURE OF MIXING RATE DURING FLOOD

Analysis presented in the preceding sections suggests that the bottom boundary layer growth rate and freshening rate are to first order a one-dimensional process. While we recognize that tidal straining, lateral circulation, and other multidimensional processes in general influence the boundary layer dynamics, based on the results above we neglect them in the following analysis.

The analysis involves the use of a structure function to model the vertical structure of the dye. The use of a structure function was necessary to avoid problems associated with noise which was amplified by taking vertical gradients. By taking advantage of the analytic properties of the structure function we can estimate the mixing rate and vertical eddy viscosity. The time-dependent, vertical distribution of dye is approximated by the similarity form

$$c(z, t) = c_o(t) f[z/\bar{\delta}(t)], \quad (8)$$

where c_o is the time-varying concentration at the base of the profile, f is a shape function (to be determined from the observations), and $\bar{\delta}$ is the time-varying scale height of the profile and proportional to the boundary layer thickness. In our Lagrangian reference frame (following the core of the dye patch) a conservation equation is written

$$\frac{dc}{dt} = -\frac{\partial}{\partial z} (\overline{c'w'}), \quad (9)$$

where the primes indicate turbulent quantities and c and w are dye concentration and vertical velocity. Integrating vertically over the boundary layer height and substituting in (8) we obtained

$$\overline{c'w'} = -\delta \frac{dc_o}{dt} \int_0^\zeta f(\zeta')\, d\zeta' + c_o \frac{d\delta}{dt} \int_0^\zeta \zeta'\, df, \quad (10)$$

where $\zeta = z/\delta$ and ζ' is a variable of integration. Integrating the second term on the right in parts we obtain

$$\overline{c'w'} = -\frac{d}{dt}(c_o \delta) \int_0^\zeta f(\zeta')\, d\zeta' + c_o \frac{d\delta}{dt} \zeta f(\zeta). \quad (11)$$

In the one-dimensional model, the first term on the right is a conservation statement of dye and is identically zero and, therefore, the vertical flux of dye is simply related to the rate of growth of the layer and the shape function. The form of the eddy diffusivity $K_z = -\overline{c'w'}/(\partial c/\partial z)$ can be easily derived from this simplification of (11):

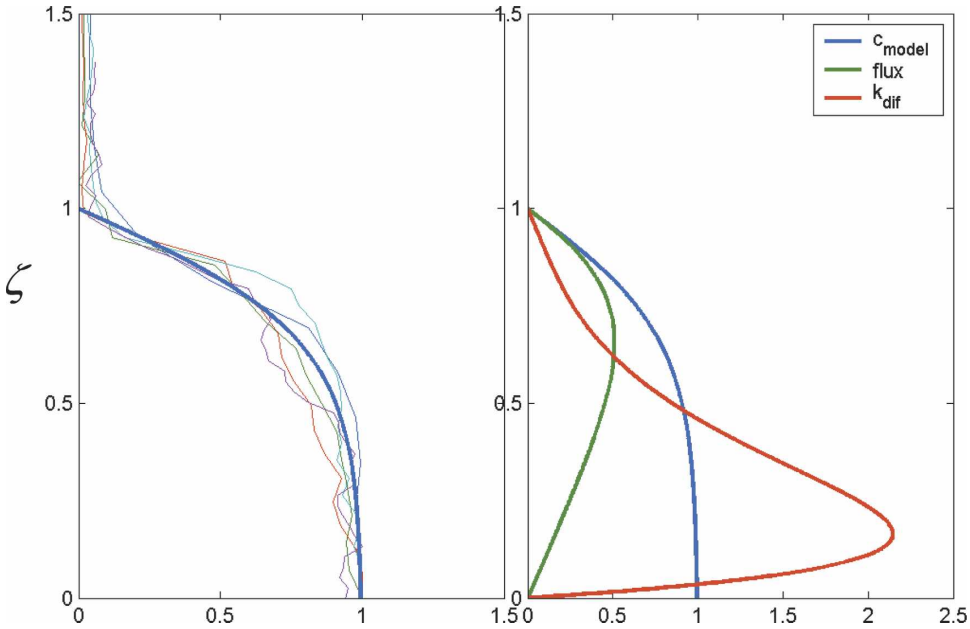

FIG. 12. (left) Vertical structure of dye observed (thin colored lines) and hyperbolic tangent. (right) Vertical structure of dye, eddy diffusivity, and vertical flux of dye based on analysis presented in section 5a(3).

$$K_z = -\delta \frac{d\delta}{dt} \zeta \frac{f(\zeta)}{f'(\zeta)}, \tag{12}$$

where f' is the vertical derivative of the shape function. Last, substituting (5) into (12) we arrive at an expression that relates the vertical eddy viscosity in the boundary layer to the friction velocity and overlying stratification:

$$K_z = -\frac{\mathrm{Ri}^{1/2}\gamma u_*^2}{N_\infty} \zeta \frac{f(\zeta)}{f'(\zeta)} = -\chi \frac{u_*^2}{N_\infty} G(\zeta), \tag{13}$$

where χ is a constant and equal to 0.61 and $G(\zeta) = \zeta f(\zeta)/f'(\zeta)$.

The function $f = \tanh[\alpha(1 - \zeta)]$ was found to be a good representation of the vertical structure of the dye (Fig. 12) with $\alpha = 3$. The value of α^{-1} represents the fraction of the boundary layer that has strong vertical gradients. Consequently, the vertical structure of the eddy viscosity in the boundary layer is

$$K_z = \chi \frac{u_*^2}{N_\infty} \zeta \frac{\tanh[\alpha(1 - \zeta)]}{\alpha \,\mathrm{sech}^2[\alpha(1 - \zeta)]}. \tag{14}$$

The vertical structure of the vertical flux of dye and the eddy diffusivity are also plotted. The greatest vertical flux occurs in the upper part of the boundary layer, but the flux abruptly goes to zero at the top of the layer. The eddy diffusivity is maximal close to the bottom, where the stratification is weakest. The diffusivity decreases markedly through the layer and goes to zero at the top of the layer.

Using estimated boundary layer growth rates during the first and third dye releases, the dimensional values of diffusivity were calculated and presented in the bottom of Table 1. Two values are reported: the maximum value, which occurs near the bottom of the boundary layer, and the value at the level of maximum dye flux (upper), which provides a characteristic value for the region of significant buoyancy flux. These values are 3.7 and 13.2 $\mathrm{cm^2\ s^{-1}}$ for the first and third releases, respectively. The maximum values are approximately five times higher, but they have little consequence for mixing due to the weak stratification near the bottom.

We found that the eddy diffusivity at the top of the boundary layer was relatively insensitive to the choice of the structure function. However the distribution of K_υ in the lower water column was very sensitive, as it depends inversely on the gradient of structure function as it approaches the boundary. A sensitivity analysis indicated that K_υ is accurately determined by this method (to within ±20%) in the upper two-thirds of the boundary layer, but it is essentially indeterminate by this method in the bottom third. While the choice of the structure function impacts estimates of the maximum eddy diffusivity it has little impact on estimates of vertical fluxes.

Last, the above analysis can be used to characterize the tidal monthly variations in the vertical buoyancy

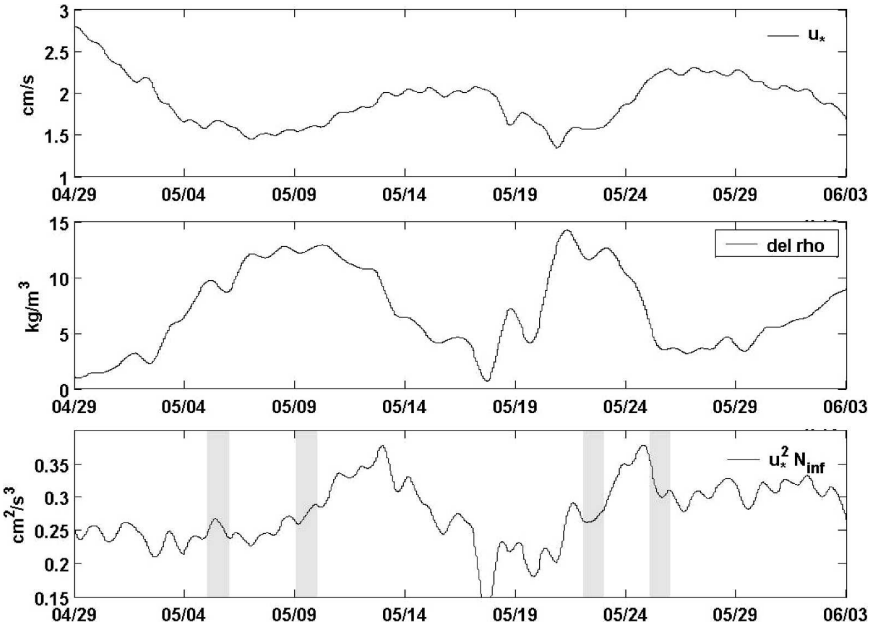

FIG. 13. (top) Bottom friction velocity during flood tide from site 4. (middle) Surface to bottom density difference from site 4. (bottom) Friction velocity squared times stratification, which is proportional to vertical salt flux [see analysis in section 4a(3)]. Gray bars indicate time of each dye experiment.

flux during the flood tide. Buoyancy flux at the top of the boundary layer is equal to $K_z N_\infty^2$, which after substituting Eq. (14) is found to be proportional to $u_*^2 N_\infty$. With data from mooring site 4 we estimated the quantity $u_*^2 N_\infty$ as a proxy for vertical salt flux. Over the spring–neap cycle friction velocity is maximum during spring tide and minimum during neap tide (Fig. 13). In contrast, stratification is maximum during neap tides and minimum during spring tide. Consequently, the vertical salt flux (or buoyancy flux) reaches a maximum during the transition from neap to spring on days 130 and 142. Following these two peaks in vertical salt flux there is a rapid decline in stratification, and despite the increase in friction velocity (and eddy viscosity) salt flux during the flood drops because of the weakened stratification. Enhanced vertical salt flux following the second spring tide is due to persistent stratification associated with the large discharge event one week earlier (Fig. 2).

b. Mechanisms influencing ebb mixing

The mixing of dye during the ebb was not the simple boundary layer entrainment process that was observed during the flood. Localized convergence of near-bottom flow caused upward advection of the dye (e.g., Fig. 4, first panel) and produced local maxima in dye that was separated from the boundary layer (e.g., Fig. 8a). As the dye patch became separated from the bottom, mixing would not necessarily result in a reduction of the salinity of the patch, but would spread the dye in salinity space. The combination of boundary layer entrainment and mixing of elevated portions of the patch caused both freshening of the patch and spreading in salinity space. During the neap-tide experiments, the mixing was weak, and upward advection often displaced maximum dye concentrations from the bottom boundary layer. This was most evident during the ebb, as seen in Fig. 8a. During the transitional experiment advective processes also displaced the peak dye concentrations off the bottom. However, as the ebb velocity intensified, a bottom boundary layer developed, within which Richardson numbers were generally below ¼ (Fig. 8a).

The contrast in mixing dynamics between the flood and the ebb appears to be due to two main factors: 1) the bottom stress was weaker during the ebb, causing relatively less intense boundary layer mixing, and 2) the influence of tidal straining competed with mixing during the ebb, reducing its effectiveness in producing a bottom mixed layer. Using the scaling of Stacey and Ralston (2005) for the influence of tidal straining on boundary layer growth, the height of the boundary layer should be limited by the relation

$$\delta \leq \sqrt{R_{\mathrm{fc}}}\,\frac{u_*}{N_x}, \tag{15}$$

where $R_{fc} \cong 0.15$ is the critical flux Richardson number and

$$N_x = \left(\frac{g}{\rho}\frac{\partial \rho}{\partial x}\right)^{0.5}$$

is a measure of the horizontal density gradient with a value of approximately 0.002 s^{-1} during this time in the Hudson. During the early and late ebb, when $u_* < 1$ cm s^{-1}, tidal straining limits the vertical extent of mixing to less than 2 m, and the overlying water column should increase in stratification due to the baroclinically induced shear. These observations suggest that the boundary layer was not as strongly limited by straining as the Stacey and Ralston relation would indicate; during maximum ebb ($u_* = 1.5$ cm s^{-1}), the observed boundary layer thickness reached 6–8 m (Fig. 8a), compared to a predicted height of 3 m. Nevertheless, the influence of tidal straining was evident in the tendency of the water column to restratify during the early and late ebb.

The occurrence of elevated maxima in dye can be explained in part by tidal straining. As the water column restratifies, patches of dye can become isolated from the bottom boundary layer. However this does not explain elevated maxima that occur soon after the injection, prior to significant vertical mixing. It appears that horizontal convergence processes are more likely to occur during the ebb than the flood, leading to vertical advective motions that carry the dye into the interior. Classical estuarine theory indicates that there should be a net vertical velocity in a partially mixed estuary (Chatwin 1976); these observations suggest that the vertical velocity is modulated within the tidal cycle, occurring preferentially during the ebb. The dynamical origins of this process are beyond the scope of this paper.

c. *Vertical buoyancy flux and the flux Richardson number*

In this final section we present estimates of the vertical turbulent buoyancy fluxes (B_f), shear production (P), and their ratio (P/B_f) or the flux Richardson number (R_f). Shear production estimates were made with the moored ACDP data, while buoyancy flux estimates are based on the analysis presented in section 4a(4). However, since this analysis is only relevant during flood, we limit our estimates of the vertical salt flux (and buoyancy flux) and the flux Richardson number to the flood. The vertical structure of salt in the bottom boundary layer during flood is similar to that of the dye, and thus we assumed a salt profile in the boundary layer as $s(z) = s_h + (s_0 - s_h)\tanh[\alpha(1 - \zeta)]$, where s_h is the salinity at the top of the boundary layer and s_0 is the bottom salinity. Using Eq. (4) to relate $d\bar{h}/dt$ to $d\bar{s}/dt$ and Eq. (11) to relate $d\bar{h}/dt$ to $|\overline{w's'}|$, where the bars represent the mean over the boundary layer, we obtain

$$\overline{|w's'|} = \bar{h}\frac{d\bar{s}}{dt}\frac{|\zeta \tanh[\alpha(1 - \zeta)]|}{|\tanh[\alpha(1 - \zeta)]|} \approx 0.4\bar{h}\frac{d\bar{s}}{dt}. \quad (16)$$

With a linearized equation of state $\rho = (1000 + \beta S)$, we estimate the depth-averaged buoyancy flux over the boundary layer as

$$|B_f| = 0.4g\frac{\beta d\bar{s}}{\rho dt}\bar{h}, \quad (17)$$

where $\beta = 0.77$ kg $(m^3$ psu$)^{-1}$. With the dye data in Figs. 7 and 9 we estimated the term $\bar{h}d\bar{s}/dt$ between each successive surveys of the patch. Here $\bar{h}$ is the mean thickness of the core of the dye patch across two successive surveys and $d\bar{s}/dt$ is estimated based on the change in the salinity of the core of the patch between surveys. With these estimates we used (17) to determine the mean buoyancy flux over the boundary layer.

Mean boundary layer shear production is estimated by assuming that stress decreases linearly from ρu_*^2 at the bottom to zero at the top of the boundary layer and that vertical shear is the maximum velocity of the mid-depth velocity jet u_∞ divided by the boundary layer depth defined by the height of the jet; that is,

$$|P| = 0.5u_*^2\frac{u_\infty}{\bar{h}}. \quad (18)$$

While these assumptions differ from the dynamics of a constant stress layer, observations presented here and in Geyer et al. (2000) suggest that both the stress and velocity profile are approximately linear in the boundary layer. Bottom friction velocity is estimated as it was done is section 4a(2).

Results from this analysis are presented in Fig. 14. In Figs. 14a and 14b the buoyancy flux estimates are multiplied by 5 so that for a flux Richardson number of 0.2 these buoyancy flux estimates are on the same scale as the shear production. On 5 May shear production during peak flood was 2×10^{-5} m^2 s^{-3} and approximately five times larger than the buoyancy flux. Data from 22 May show a similar relationship with peak shear production around 5×10^{-5} m^2 s^{-3} and buoyancy flux at 10^{-5} m^2 s^{-3}. A scatterplot between all estimates of shear production and buoyancy flux (Fig. 14c) has an $r^2 = 0.64$ and regression of 0.14. The regression represents an estimate of the flux Richardson number. Given the standard error of the fit and 90% confidence limits our analysis places the flux Richardson number between 0.1–0.18. Since the maximum value that the flux

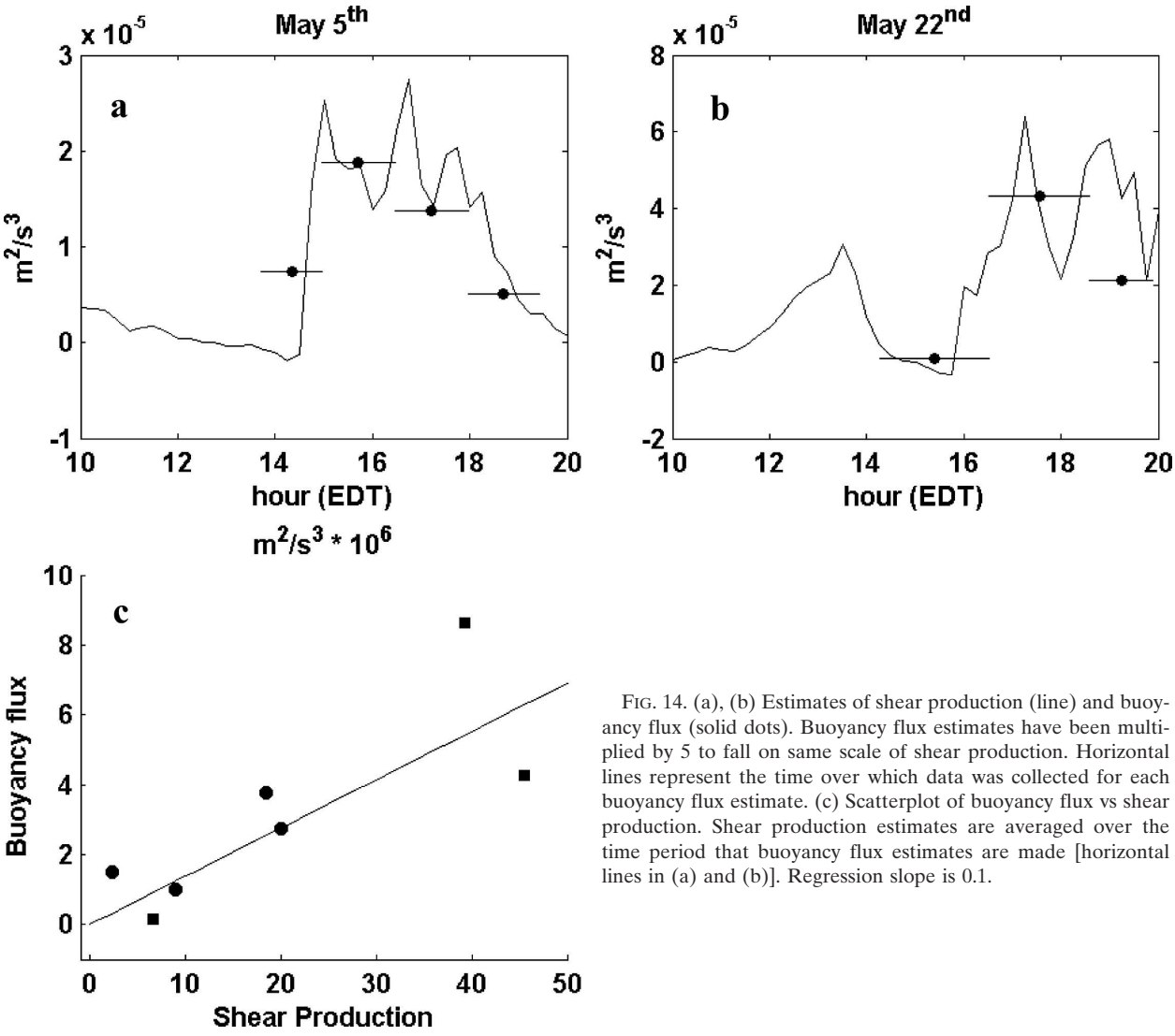

FIG. 14. (a), (b) Estimates of shear production (line) and buoyancy flux (solid dots). Buoyancy flux estimates have been multiplied by 5 to fall on same scale of shear production. Horizontal lines represent the time over which data was collected for each buoyancy flux estimate. (c) Scatterplot of buoyancy flux vs shear production. Shear production estimates are averaged over the time period that buoyancy flux estimates are made [horizontal lines in (a) and (b)]. Regression slope is 0.1.

Richardson number can take in stratified turbulence is 0.2 (Tennekes and Lumley 1982), these estimates of the flux Richardson number suggests that shear production in the boundary layer is efficient in driving a vertical buoyancy flux.

Using our expression for the vertical eddy diffusivity (14) and the structure function for the density profile in the boundary layer, $\rho = \rho_h + \Delta\rho \tanh[\alpha(1 - \zeta)]$, the model predicts a buoyancy flux (B_f)

$$B_f(\zeta) = \frac{g}{\rho} k_v \frac{\partial \rho}{\partial z} = \chi \frac{N_{\mathrm{BL}}^2}{N_\infty} u_*^2 \zeta \tanh[\alpha(1 - \zeta)], \tag{19}$$

where

$$N_{\mathrm{BL}} = \frac{g\Delta\rho}{\rho\bar{h}}$$

and $\Delta\rho$ are the buoyancy frequency and density difference across the boundary layer, respectively. Note that N_∞ occurs at the top of the boundary layer where the density gradient is maximum, and with the use of the structure function we find that $N_\infty^2 = \alpha N_{\mathrm{BL}}^2$. Thus averaging (19) over the boundary layer we find

$$|B_f| = 0.063 N_\infty u_*^2 = 0.11 N_{\mathrm{BL}} u_*^2. \tag{20}$$

Using the values in Table 1 for N_∞ and u_* (19) predicts buoyancy fluxes of 1.3×10^{-6} and 2.0×10^{-6} m^2 s^{-3} for 5 and 22 May, respectively. Using the maximum values for u_* on those days based on Fig. 10 (2 cm s^{-1} for 5 May and 3 cm s^{-1} for 6 May) yields buoyancy fluxes of 2.8×10^{-6} and 4.3×10^{-6} m^2 s^{-3} for those two days. These values fall within the range of measured values as

shown in Fig. 14c. Last, equating (20) with (18) times R_f, both representing expressions for the boundary layer mean buoyancy, we find

$$0.22\frac{N_{\mathrm{BL}}h}{u_\infty} = 0.22\sqrt{\mathrm{Ri}_{\mathrm{BL}}} = R_f. \tag{21}$$

Richardson number estimates made in the boundary layer on 5 and 22 May are approximately 0.5 and 0.25, respectively (Figs. 5 and 8) and correspond to a flux Richardson number, according to (21), of 0.16 and 0.11. Both estimates, made with (21), fall within the error bars of the flux Richardson number estimate that we made with the experimental data (Fig. 14c) and suggest that the coefficients derived for the boundary layer model are essentially correct.

5. Conclusions

A series of dye studies conducted in the Hudson River estuary during May 2002 elucidated bottom boundary layer mixing processes, their rates, and temporal variability over tidal and fortnightly time scales. Results emphasize that diapycnal mixing occurs through entrainment generated by bottom boundary layer turbulence. During neap tides there is a strong tidal asymmetry in salt flux with stronger fluxes during the flood. Approaching the spring–neap transition this asymmetry is reduced. During flood the bottom boundary layer is clearly defined by the dye patch, which mixes up to the top of the boundary layer, and by the depth of a subsurface velocity maximum. The growth of the boundary layer during flood is primarily due to entrainment with minimal contribution to flow convergence or tidal straining. Observed boundary layer growth rates during flood are consistent with a 1D entrainment model (Trowbridge 1992). We presented a 1D model that provides a expression for vertical structure of eddy viscosity in the boundary layer, proportional to u_*^2/N_∞, and that the mean buoyancy flux over the boundary layer is equal to $0.11N_{\mathrm{BL}}u_*^2$. The 1D model was used to estimate vertical turbulent salt flux over the neap–spring cycle and suggests that maximum vertical salt flux occurs as tidal range is increasing midway between neap and spring tide conditions. Estimates of the flux Richardson number in the boundary layer made both with the model and the observations agree and lie between 0.1–0.18. Last, tidal straining limits its boundary layer height during ebb, as suggested by Stacey and Ralston (2005).

Acknowledgments. The work was supported by the National Science Foundation Grant OCE00-95972 (W. Geyer, J. Lerczak), OCE00-99310 (R. Houghton), and OCE00-95913 (R. Chant, E. Hunter). We thank two anonymous reviewers for their highly constructive comments that helped to significantly improve earlier versions of this paper. We thank John Lipscomb and the Hudson River Riverkeeper for their tireless and enthusiastic efforts in the field program and John Trowbridge for providing critical insight in the boundary layer analysis.

REFERENCES

Chant, R. J., and R. E. Wilson, 1997: Secondary circulation in a highly stratified channel. *J. Geophys. Res.,* **102,** 23 207–23 215.

——, and ——, 2000: Internal hydraulics and mixing in a highly stratified estuary. *J. Geophys. Res.,* **105,** 14 215–14 222.

Chatwin, P. C., 1976: Some remarks on the maintenance of the salinity distribution in estuaries. *Estuarine Coastal Mar. Sci.,* **4,** 555–566.

Geyer, W. R., J. H. Trowbridge, and M. M. Bowen, 2000: The dynamics of a partially mixed estuary. *J. Phys. Oceanogr.,* **30,** 2035–2048.

Houghton, R. W., C. E. Tilburg, R. W. Garvine, and A. Fong, 2004: Delaware River plume response to a strong upwelling-favorable wind event. *Geophys. Res. Lett.,* **31,** L07302, doi:10.1029/2003GL018988.

Jay, D. A., and D. J. Smith, 1990: Circulation, density distribution and neap–spring transitions in the Columbia River estuary. *Prog. Oceanogr.,* **25,** 81–112.

Kantha, L. H., O. M. Phillips, and R. S. Azad, 1977: On turbulent entrainment at a stable density interface. *J. Fluid Mech.,* **79,** 753–768.

Kato, H., and O. M. Phillips, 1969: On the penetration of a turbulent layer into stratified fluid. *J. Fluid Mech.,* **37,** 643–655.

Ledwell, J. R., A. J. Watson, and C. S. Law, 1993: Evidence of slow mixing across the pycnocline from an open ocean tracer release experiment. *Nature,* **364,** 701–703.

——, T. F. Duda, M. A. Sundermeyer, and H. E. Seim, 2004: Mixing in a coastal environment: 1. A view from dye dispersion. *J. Geophys. Res.,* **109,** C10013, doi:10.1029/2003JC002194.

Lerczak, J., W. R. Geyer, and R. J. Chant, 2006: Mechanisms driving the time-dependent salt flux in a partially stratified estuary. *J. Phys. Oceanogr.,* **36,** 2296–2311.

Lu, Y. Y., R. G. Lueck, and D. Y. Huang, 2000: Turbulence characteristics in a tidal channel. *J. Phys. Oceanogr.,* **30,** 855–867.

Monismith, S. G., W. Kimmerer, J. R. Burau, and M. T. Stacey, 2002: Structure and flow-induced variability of the subtidal salinity field in northern San Francisco Bay. *J. Phys. Oceanogr.,* **32,** 3003–3019.

Osborne, T. R., 1980: Estimates of the local rate of vertical diffusion from dissipation measurements. *J. Phys. Oceanogr.,* **10,** 83–89.

Peters, H., 1997: Observations of stratified turbulent mixing in an estuary: Neap-to-spring variations during high river flow. *Estuarine Coastal Shelf Sci.,* **45,** 69–88.

——, and R. Bokhorst, 2000: Microstructure observations of turbulent mixing in a partially mixed estuary. Part I: Dissipation rate. *J. Phys. Oceanogr.,* **30,** 1232–1244.

Price, J. F., R. A. Weller, and R. Pinkel, 1986: Diurnal cycling: Observations and models of the upper ocean response to

diurnal heating, cooling and wind mixing. *J. Geophys. Res.,* **91,** 8411–8427.

Rippeth, T. P., E. Williams, and H. J. Simpson, 2002: Reynolds stress and turbulent energy production in a tidal channel. *J. Phys. Oceanogr.,* **32,** 1242–1251.

Simpson, J. H., J. Brown, J. Matthews, and G. Allen, 1990: Tidal straining, density currents and stirring in the control of estuarine stratification. *Estuaries,* **13,** 125–132.

——, H. Burchard, N. R. Fisher, and T. P. Rippeth, 2002: The semi-diurnal cycle of dissipation in a ROFI: Model-measurement comparisons. *Cont. Shelf Res.,* **22,** 1615–1628.

Stacey, M. T., and D. K. Ralston, 2005: The scaling and structure of the estuarine bottom boundary layer. *J. Phys. Oceanogr.,* **35,** 55–71.

——, S. G. Monismith, and J. R. Burau, 1999: Measurements of Reynolds stress profiles in unstratified tidal flow. *J. Geophys. Res.,* **104,** 10 933–10 949.

Sundermeyer, M. A., and J. R. Ledwell, 2001: Lateral dispersion over the continental shelf: Analysis of dye-release experiments. *J. Geophys. Res.,* **106,** 9603–9622.

Tennekes, H., and J. L. Lumley, 1982: *A First Course in Turbulence*. MIT Press, 300 pp.

Trowbridge, J. H., 1992: A simple description of the deepening and structure of a stably stratified flow driven by a surface stress. *J. Geophys. Res.,* **97C,** 15 529–15 543.

——, W. R. Geyer, M. M. Bowen, and A. J. Williams III, 1999: Near-bottom turbulence measurements in a partially mixed estuary: Turbulent energy balance, velocity structure, and along-channel momentum balance. *J. Phys. Oceanogr.,* **29,** 3056–3072.